

Dirac and chiral spin liquids on spin-1/2 square-lattice Heisenberg antiferromagnet

Hui-Ke Jin,^{1,*} Hong-Hao Tu,² and Ya-Hui Zhang³

¹*School of Physical Science and Technology, ShanghaiTech University, Shanghai 201210, China*

²*Ludwig-Maximilians-Universität München, 80333 Munich, Germany*

³*William H. Miller III Department of Physics and Astronomy, Johns Hopkins University, Baltimore, Maryland, 21218, USA*

(Dated: December 2, 2024)

We revisit the challenging problem of identifying the quantum spin liquid candidate in the spin-1/2 J_1 - J_2 Heisenberg antiferromagnet on the square lattice. By integrating the Gutzwiller-guided density matrix renormalization group method with analytical analyses, we present clear evidence that the ground state is a Z_2 Dirac spin liquid. This state can be efficiently described by a Gutzwiller-projected parton theory characterized by its projective symmetry group. To distinguish the difference between the projected Z_2 and $U(1)$ parton state, we investigate the chiral spin liquid ground states as topological orders by incorporating a J_χ term into the J_1 - J_2 model and observe a transition from a Z_2 chiral spin liquid to a $U(1)_2$ chiral spin liquid as J_χ increases.

Introduction—The discovery of high- T_c superconductivity has motivated significant interest in the research on quantum spin liquids (QSL) [1–6]. Over the past few decades, the field of QSL has garnered significant attention, driven by the discovery of emergent long-range entanglement, fractional quasiparticles, and gauge fields [7–12]. One of the prototypical and concrete models for QSL is the spin-1/2 J_1 - J_2 antiferromagnetic (AFM) Heisenberg model on the square lattice (hereafter referred to as the J_1 - J_2 model), where J_1 and J_2 represent the AFM exchanges on the first and second nearest neighbor (NN) bonds, respectively.

It is generally accepted that the J_1 - J_2 model exhibits a paramagnetic phase in the intermediate regime $J_2 \approx 0.5J_1$, where the interplay of quantum fluctuation and geometric frustration destroys the long-range Néel order at small J_2 . However, despite tremendous endeavors by various approaches [13–61], the ground state of this paramagnetic phase has been elusive. Possible candidates include (columnar or plaquette) valence-bond solid (VBS) [14–30], gapless QSL [31–41], and gapped QSL [42]. Besides, a recent study suggests the absence of such a paramagnetic phase [43]. Overall, the nature of the intermediate J_2 regime remains highly debated.

In this work, we revisit this challenging problem and clarify the nature of ground states in the J_1 - J_2 model. We use the density matrix renormalization group (DMRG) method [62–64] and analytical analyses to unveil a Dirac QSL ground state. The key observation is that such a Dirac QSL indeed can be described by a Gutzwiller-projected Z_2 parton state within the framework of projective symmetry group (PSG) [65]. We emphasize that our numerical results, based on the newly developed method [66], demonstrate an efficient approach to mitigating finite-size effects generally encountered in DMRG simulations. The Z_2 QSL also indicates a possible Z_2 chiral spin liquid (CSL) phase in the vicinity of the J_1 - J_2 model. The topological order of this Z_2 CSL is distinct from the Kalmeyer-Laughlin state [67, 68]. To explore such a potential topological order, we incorporate a spin chirality term J_χ

into the J_1 - J_2 model. As J_χ increases, we observe a transition from the Z_2 CSL phase to a usual $U(1)$ CSL phase.

Model and setup— We study the spin-1/2 J_1 - J_2 model on the square lattice, defined as

$$\mathcal{H} = J_1 \sum_{\langle ij \rangle_1} \vec{S}_i \cdot \vec{S}_j + J_2 \sum_{\langle ij \rangle_2} \vec{S}_i \cdot \vec{S}_j, \quad (1)$$

where \vec{S}_i is the vector of three spin-1/2 operators and $\langle ij \rangle_{1(2)}$ runs over all the 1st (2nd) NN bonds. The ground-state phase diagram of the J_1 - J_2 model has been extensively explored in previous works [28, 35, 40, 42], as sketched in Fig. 1(a). In this study, we focus on the paramagnetic regime supporting QSLs by restricting the model parameters to $J_2 = 0.5J_1$, corresponding to the maximally frustrated point in the classical limit.

The space group (SG) symmetry of the J_1 - J_2 model is pivotal for the following analysis. As illustrated in Fig. 1(a), the SG is generated by two translations T_x and T_y , a C_4 lattice rotation around the out-of-plane z -axis, and a parity symmetry P_y (reflection) across the x -axis. Besides the SG symmetries, Eq. (1) is also invariant under the time-reversal symmetry (TRS) $\mathcal{T}^2 = 1$ (for an even number of spins). Combining \mathcal{T} with the SG yields the entire symmetry group for the J_1 - J_2 model; see Supplementary Material [69] for further details.

To demonstrate the Z_2 Dirac QSL we introduce fermionic parton operators $f_{i,s}$, with $s = 1, 2$ being the spin up and down index. Then, spin-1/2 operators can be written in a fermion bilinear form $S_i^a = \frac{1}{2} \sum_{s,s'} f_{i,s}^\dagger \sigma_{ss'}^a f_{i,s'}$, where σ^a ($a = x, y, z$) are three Pauli matrices. This parton representation has an $SU(2)$ gauge redundancy, as straightforwardly evidenced in the framework of Nambu spinor $\psi_i = (f_{i,\uparrow}, f_{i,\downarrow})^T$. With simple algebra [69], one can show that the spin operators are invariant under arbitrary $SU(2)$ gauge rotations $\psi_i \rightarrow G_i \psi_i$, where G_i is a *local* $SU(2)$ transformation. This redundancy indicates an enlarged Hilbert space with unphysical double- and non-occupancy states. The physical Hilbert space is restored by imposing a local single-occupancy constraint, $\sum_s f_{i,s}^\dagger f_{i,s} = 1$. In practice, this procedure, known as Gutzwiller projection, is carried out by exactly projecting out unphysical states, thereby eliminating redundant gauge fluctuations.

*Electronic address: jinhk@shanghaitech.edu.cn

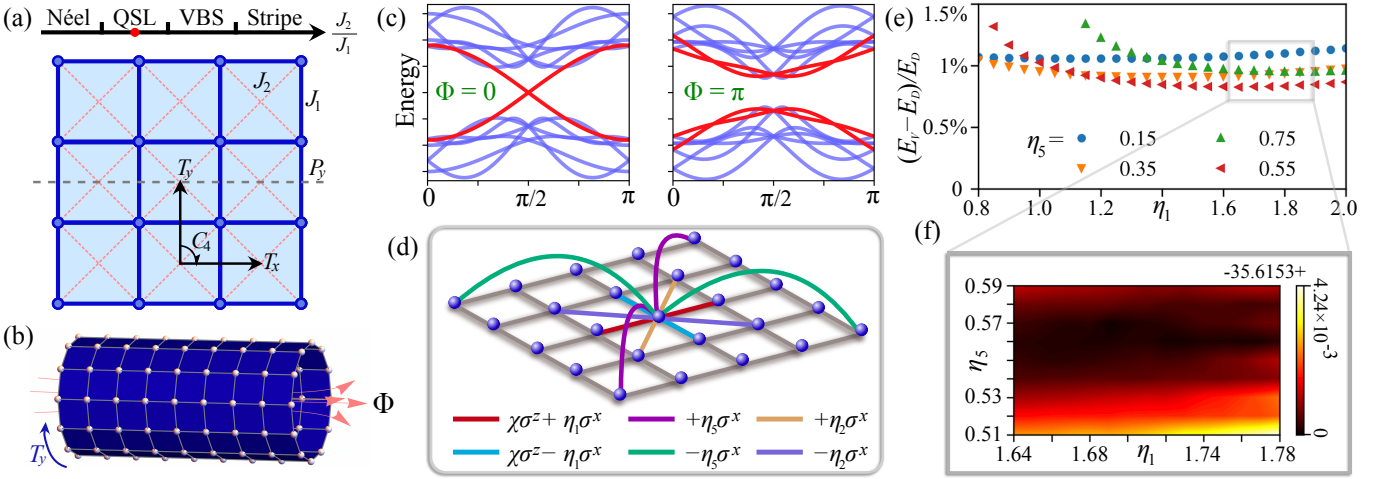


FIG. 1: The J_1 - J_2 model and Z_2 Dirac QSL. (a) Lattice symmetries and ground-state phase diagram of the J_1 - J_2 model on the square lattice. The red dot denotes the point $J_2/J_1 = 0.5$ being of interest here. (b) The square lattice is wrapped onto a cylinder, where the \hat{y} -direction is periodic, and the \hat{x} -direction remains open. The partons experience an emergent global gauge flux Φ , which effectively introduces a phase factor of $e^{i\Phi}$ for the partons on the boundary. (c) For the Z_2 DSL ansatz on a YC8 cylinder ($\eta_2 = 0$), the Dirac cones at $\pm(k_x/2, k_y/2)$ can manifest only when $\Phi = 0$, while they are gapped a $\Phi = \pi$ flux. (d) The projective symmetry group for the Z_2 Dirac QSL with the 1st, 2nd, and 5th NN parton parameters; see Eq. (3). (e, f) The variational energy E_V for Z_2 DSL on a YC6 cylinder with length $L_x = 12$ with respect to the DMRG-obtained energy $E_D \approx -35.91$ ($\chi_D = 8000$). The contour plot (f) provides a zoom-in view of the variational energy landscape. For $\eta_2 = 0$, the best $E_V \approx -35.615$ is obtained at $(\eta_1, \eta_5) = (1.7, 0.57)$ with $\chi_S = 4000$. Further optimizing η_2 leads to $E_V \approx -35.632$.

This parton representation allows us to systematically construct QSL states [65] using the following parton mean-field Hamiltonian:

$$H_{MF} = \sum_{ij} (\psi_i^\dagger \mu_{ij} \psi_j + \text{h.c.}). \quad (2)$$

Here the mean-field ansatz $\mu_{ij} = \mu_{ji}^\dagger$, which fully characterizes the physical properties of QSL, takes a general form of $\mu_{ij} = i\chi'_{ij}\sigma^0 + \eta_{ij}\sigma^x + \eta'_{ij}\sigma^y + \chi_{ij}\sigma^z$ with χ 's and η 's being real parameters. Note that, due to the $SU(2)$ gauge structure, the hopping terms of partons (σ^z and σ^0 terms) can be transformed into the singlet pairings of partons (σ^x and σ^y terms) by a certain gauge transformation, and vice versa. The QSL state as a many-body spin wave function is obtained by applying Gutzwiller projection to the parton ground state of Eq. (2). Because of the $SU(2)$ gauge redundancy in parton representation, the form of mean-field ansatz μ_{ij} is gauge-dependent and is transformed under gauge rotations as $\mu_{ij} \rightarrow G_i \mu_{ij} G_j^\dagger$ [65]. It indicates that, after exactly implementing the Gutzwiller projection, two seemingly different ansatzs μ_{ij} and μ'_{ij} can lead to the same QSL state if there exists a set of $\{G_i\}$ such that $\mu_{ij} = G_i \mu'_{ij} G_j^\dagger$. Moreover, the form of a symmetric ansatz is allowed to vary under symmetry transformations in SG — as long as the transformed ansatz is gauge equivalent to its original form [69]. Thus, when characterizing a QSL, one must also specify its projective symmetries within the framework of PSG [65].

Z_2 parton ansatz— As a key finding, we report that the QSL phase in the J_1 - J_2 model is a Z_2 Dirac QSL described by the

mean-field ansatz as illustrated in Fig. 1(d)

$$\begin{aligned} \mu_{i,i+\hat{x}} &= \chi\sigma^z + \eta_1\sigma^x, & \mu_{i,i+\hat{y}} &= \chi\sigma^z - \eta_1\sigma^x \\ \mu_{i,i+2(\hat{x}+\hat{y})} &= \eta_5\sigma^x, & \mu_{i,i+2(\hat{x}-\hat{y})} &= -\eta_5\sigma^x, \\ \mu_{i,i+\hat{x}+\hat{y}} &= \eta_2\sigma^x, & \mu_{i,i+\hat{x}-\hat{y}} &= -\eta_2\sigma^x, \end{aligned} \quad (3)$$

where we fix $\chi_1 \equiv \chi = 1$ and treat η_1 , η_2 , and η_5 on the 1st, 2nd, and 5th NN bonds as variational parameters, respectively. The mean-field Hamiltonian in Eq. (3), in addition to its Z_2 -type gauge fluctuations, manifests Dirac-type excitations at momenta $\mathbf{k} = (\pm\pi/2, \pm\pi/2)$ when $\eta_2 = 0$, while a finite value of η_2 shifts the Dirac cones away from the commensurate point. Thus, we denote this ansatz as Z_2 DSL. The PSG solution for the Z_2 DSL is detailed in the Supplementary Material [69]. In accordance with the PSG, one can find that this Z_2 DSL turns into a $U(1)$ Dirac QSL for $\eta_5 = \eta_2 = 0$ [69], wherein Eq. (3) is equivalent to the staggered-flux state given by [6, 70],

$$H_{SF} = \sum_{\langle ij \rangle_{1,s}} \exp[i(-1)^{i_x+j_y} \Theta] f_{i,s}^\dagger f_{j,s} + \text{h.c.},$$

where $\tan \Theta = \eta_1/\chi_1$ and i_a ($a = x, y$) is the lattice index of site i in a direction. Furthermore, the staggered-flux state preserves the $SU(2)$ gauge symmetry at the special point of $\eta_1 = \chi_1$. It indicates that if either η_2 or η_5 is zero, the Z_2 DSL ansatz with $\eta_1 = \chi_1$ actually corresponds to a $U(1)$ Dirac QSL rather than a Z_2 one. The importance of η_2 for a Z_2 QSL has been investigated previously [71, 72], as the η_2 term can be naturally anticipated from a straightforward mean-field analysis of the J_1 - J_2 model. Rather than η_2 , later we will see that the η_5 term, which is unexpected from a mean-field decoupling perspective, plays a more important role in the J_1 - J_2

model. Furthermore, the PSG solution also implies that other possible terms like $i\sigma^0$ and σ^y on the bonds along the \hat{x} -, \hat{y} -, and $\hat{x} \pm \hat{y}$ -directions are forbidden due to the parity symmetries.

The energetics and certain correlation functions of Z_2 DSL have already been explored using variational Monte Carlo [31, 33, 38]. Here, we shall adopt newly developed methods based on matrix product state (MPS) [66, 73–77], which allow us to compute wave function fidelity and entanglement entropy. To perform MPS calculations, we wrap the square lattice onto a finite-circumference cylinder and impose a periodic boundary condition (PBC) on the spin-1/2 variables, as shown in Fig. 1(b). The cylinder is denoted as YCL_y , where L_y represents the circumference, and its length along the open boundary direction is L_x . Strictly speaking, this cylindrical geometry preserves the parity symmetry P_y but breaks the C_4 symmetry into a twofold C_2 rotation symmetry.

Due to the PBC for the spin variables, the fermionic partons placed on cylinders are coupled to an emergent global gauge flux Φ threading through the cylinder [see Fig. 1(b)]. This global flux effectively twists the boundary condition for the partons along the \hat{y} direction, i.e., shifting the allowed momenta of partons to $k_y = (2n\pi + \Phi)/L_y$, $n = 1, \dots, L_y$. The product of parity and rotation symmetries $P_y C_2$ requires $\Phi = 0$ and $\Phi = \pi$, corresponding to periodic and antiperiodic boundary conditions, respectively.

In the thermodynamic limit, the effect of Φ on local observables vanishes as $L_y \rightarrow \infty$. However, the global flux Φ plays an important role in cylindrical systems, as it corresponds to different crystal momenta cutting through the Brillouin zone. By fixing the gauge for the Z_2 DSL as in Eq. (3) (without loss of generality we make $\eta_2 = 0$), the allowed momenta exactly cut the Dirac cones of Z_2 DSL at $\pm(\pi/2, \pi/2)$ only when $\Phi = 0$ ($\Phi = \pi$) for $L_y/2$ being even (odd). For instance, the one-dimensional band structure for Z_2 DSL on a YC8 cylinder is illustrated in Fig. 1(c), where it exhibits a (finite-size) band gap for $\Phi = \pi$, in contrast to the appearance of Dirac cones for $\Phi = 0$. It indicates that even if the J_1 - J_2 model is described by a gapless Z_2 DSL ansatz, it may manifest spurious characteristics of gapped states when placed on certain types of finite cylinders. Consequently, one may misidentify the J_1 - J_2 model as a gapped QSL or other states when focusing only on local quantities like energetics and (short-distance) correlation functions.

Numerical results— Apart from the parton ansatz, we also employ the DMRG method to simulate the J_1 - J_2 model directly. The U(1) quantum number corresponding to S^z conservation is explicitly used, with bond dimensions for preparing MPS and performing DMRG calculations denoted by χ_S and χ_D , respectively. The DMRG calculations are initialized with randomly generated MPSs or Gutzwiller projected parton states [66].

We treat the global flux $\Phi = 0$ and π as a discrete parameter and compare the variational energy E_V of Z_2 DSL in both flux sectors. For the same variational parameters, we find that the lower-energy sector is always the one wherein the Dirac cones are avoided. By filling the single-particle energy levels below the Dirac cones, the “gapped” sector gains energy of

$\delta E_V \sim v_F/L_y$ by avoiding cutting the Dirac cones, where v_F is the spinon Fermi velocity. Note that this scenario also explains why the singlet energy gap in the J_1 - J_2 model scales as L_y^{-1} [35, 43], since the parton band gap introduced by Φ closes proportionally as $v_F \delta k_y \propto v_F L_y^{-1}$.

In the following, we concentrate on the “gapped” sector and optimize the parameters η_1 and η_5 of Z_2 DSL by minimizing the variational energy E_V . After a careful search in the parameter space, as demonstrated in Fig. 1(e-f), we find that the lowest energy E_V is always achieved with a finite η_5 . For instance, the optimal values of η_5 are 0.42, 0.57, and 0.58 for YC4, YC6, and YC8 cylinders, respectively. These values are consistent with variational Monte Carlo results [33, 38]. We find that the quality of the Z_2 DSL ansatz is not sensitive to $\pm\eta_2\sigma^x$ terms on the 2nd NN bonds [see Fig. 1(d)]. This term preserves the PSG of Z_2 DSL and shifts the Dirac cone away from $(\pm\pi/2, \pm\pi/2)$ (with our gauge choice). Although the energy can be slightly improved with a finite $\eta_2 \approx 0.04$, we set $\eta_2 = 0$ in discussions below for simplicity.

We emphasize that the presence of finite η_5 , besides contributing to additional energy gain, is also essential for breaking the SU(2) gauge structure down to a Z_2 one. As mentioned above, for $\eta_5 = \eta_2 = 0$, Z_2 DSL is equivalent to the U(1) staggered-flux state. Nevertheless, our numerics clearly demonstrate that for the J_1 - J_2 model (i) the optimal value of η_5 (η_2) is finite (close to zero) and (ii) the optimal value of η_1 is far away from the special SU(2) point of $\eta_1 = \chi_1$, as shown in Fig. 1(e). Overall, all these results suggest that the J_1 - J_2 model is more likely to support a gapless Z_2 QSL rather than a U(1) QSL in the 2D limit.

We also perform DMRG calculations initialized with randomly generated MPS and Z_2 DSL ansatz, both of which converge to the same unbiased ground-state energy E_D . In contrast, utilizing a Z_2 DSL initial state significantly reduces the wall time required to achieve converged energy by half, in comparison to starting with a random MPS [69]. Moreover, the relative difference between E_D and variational energy E_V is as small as 0.8%, as shown in Fig. 1(e). The validity of the Z_2 DSL ansatz can be further confirmed by calculating the wave function fidelity $F = |\langle \Psi_{\text{DMRG}} | \Psi_{Z_2\text{DSL}} \rangle|$. Notably, the per-site fidelity achieves a high value of approximately

$$\tilde{f} \equiv F^{1/L_x L_y} \approx 99.86\%,$$

which turns out to be unchanged with L_x and even L_y [69]. For instance, the fidelity on YC6 and YC8 cylinders with $L_x = 12$ read $F \approx 0.91$ and $F \approx 0.87$, respectively. This high fidelity provides clear evidence that the ground state of the J_1 - J_2 model is indeed a Z_2 Dirac QSL described by our parton ansatz. We also numerically examine the SU(2) π -flux state [65] which also has Dirac spinon excitations. However, our results on energetics and wave function fidelity are not in favor of such an SU(2) π -flux state as the candidate ground state of the J_1 - J_2 model [69].

CSLs by spin chirality— The presence of Z_2 DSL suggests that incorporating a chiral term into the J_1 - J_2 model can break time-reversal symmetry and lead to an unusual Z_2 CSL ground

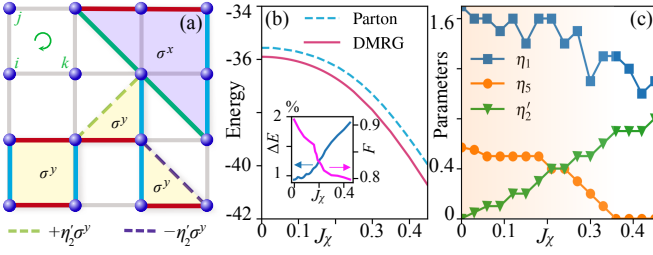


FIG. 2: The Z_2 and $U(1)$ CSLs in the J_1 - J_2 - J_χ model. (a) The sites i , j , and k indicate the chiral terms discussed in Eq. (4). The dashed off-diagonal lines denote η'_2 terms in Eq. (5b). The enclosed flux within the elementary square, elementary triangular, and big triangular plaquettes sustains $U(1)$, $U(1)$, and Z_2 gauge fluctuations, respectively. (b) The best variational parton energy ($\chi_S=2000$) and DMRG energy ($\chi_D=4000$) as functions of J_χ on a YC6 cylinder with $L_x = 12$. Inset: The relative energy difference (left axis), $\Delta E = (E_D - E_V)/E_D$ slowly increases with J_χ . The wave function fidelity (right axis), $F = |\langle \Psi_{\text{DMRG}} | \Psi_{\text{CSL}} \rangle|$, as a function of J_χ . (c) The optimized parameters as functions of J_χ . For $J_\chi \gtrsim 0.35$, η_5 vanishes, and the system undergoes a transition from a Z_2 CSL to a $U(1)$ CSL.

state. To this end, we consider the J_1 - J_2 - J_χ model

$$\mathcal{H}_\chi = \mathcal{H} + J_\chi \sum_{ijl \in \Delta} \vec{S}_i \cdot (\vec{S}_j \times \vec{S}_k), \quad (4)$$

where the sites i , j and k in each triangle $ijl \in \Delta$ follow the same clockwise direction [see Fig. 2(a)]. Besides the \mathcal{T} symmetry, the lattice parity symmetry P_y is also broken explicitly by the chiral J_χ term. Nevertheless, the rotation symmetry C_4 is preserved in the presence of J_χ . This chiral term can gap out the Dirac cones in Z_2 DSL [78–82], leading to gapped CSL ground states characterized by topological order [83].

When J_χ is relatively small, one can intuitively expect that the Z_2 DSL ansatz incorporating TRSB perturbations could be a promising candidate for the ground state of Eq. (4). Thus, several additional terms, which were ruled out by the PSG of Z_2 DSL [69], should be taken back as the perturbations for the Z_2 DSL. Thus, apart from the terms in Eq. (3), we introduce an additional set of parameters for the CSL regime:

$$\mu'_{i,i+\hat{x}} = i\chi'_1\sigma^0 + \eta'_1\sigma^y, \quad \mu'_{i,i+\hat{y}} = -i\chi'_1\sigma^0 - \eta'_1\sigma^y, \quad (5a)$$

$$\mu'_{i,i+\hat{x}\pm\hat{y}} = i\chi'_2\sigma^0 \pm \eta'_2\sigma^y. \quad (5b)$$

In the gauge we have chosen, η'_1 and η'_2 are the $id_{x^2-y^2}$ and id_{xy} pairings on the 1st and 2nd NN bonds, respectively. After a careful investigation, we find that only the η'_2 term significantly improves the variational energy with varying J_χ [69]. Therefore, only η'_2 among the aforementioned parameters is pivotal in mimicking the low-energy physics of the J_1 - J_2 - J_χ model. Indeed, η'_2 is an effective mass term for the Dirac fermions in the Z_2 Dirac QSL. Consequently, we proceed to investigate potential CSL phases by focusing on the CSL ansatz, which is a Gutzwiller projected $d + id$ state with variational parameters $(\eta_1, \eta'_2, \eta_5)$.

For a given value of J_χ , we calculate the ground-state energy of the J_1 - J_2 - J_χ model using DMRG as well as the variational energy of the Gutzwiller projected parton states

parametrized by three parameters $(\eta_1, \eta'_2, \eta_5)$. We observed that DMRG calculations initialized with parton states and random MPSs give rise to the same converged ground states. As shown in Fig. 2(b), despite a gradual and slow increase with J_χ , the relative energy difference always remains below 2% for $J_\chi < 0.4$. We also computed the wave function fidelity F between the state obtained by DMRG and the Gutzwiller projected parton state on a YC6 cylinder with $L_x = 12$. As J_χ increases, F undergoes an almost linear decrease from $F \approx 0.91$ (for $J_\chi = 0$) to $F \approx 0.81$ ($J_\chi = 0.3$). Subsequently, its value slowly decreases or fluctuates around 0.8 for $J_\chi < 0.45$, as shown in the inset of Fig. 2(b). Overall, in the regime of our interest, the per-site fidelity is always larger than 99.68%, indicating that the whole CSL phase can be well described by our CSL parton ansatz, in particular for $J_\chi < 0.2$.

We uncover a possible phase transition within the CSL regime, as revealed by the evolution of the optimal parton parameters with J_χ . As shown in Fig. 2(c), η_5 (the d_{xy} pairing on the 5th NN bonds) stays at a plateau value around 0.5 when $J_\chi \lesssim 0.2$, and subsequently declines to zero as $J_\chi \approx 0.35$. Meanwhile, η'_2 , representing the id_{xy} pairing on the 2nd NN bonds, exhibits an approximately linear increase with the rise in J_χ . Finally, η_1 always remains finite on the 1st bond. The vanish of η_5 indicates a phase transition from a Z_2 CSL to a $U(1)$ CSL. To see this, we carefully examine the nonzero $SU(2)$ gauge fluxes [65, 69] in our CSL ansatz. As shown in Fig. 2(a), the $SU(2)$ gauge fluxes around an elementary square and/or an elementary triangle manifest as $a\sigma^0 + b\sigma^y$, where a and b are complex numbers. Since they are invariant under arbitrary $U(1)$ gauge transformations generated by σ^y , the set of parameters (η_1, η'_2) indeed corresponds to a $U(1)$ CSL. However, the gauge flux around the large triangle [see Fig. 2(a)] has a form of $\sim \eta_5\sigma^x$ and thereby only the Z_2 number $\pm\sigma^0$ can simultaneously commute the two fluxes proportional to σ^y and σ^x , respectively. Consequently, a finite value of η_5 changes such a $U(1)$ CSL into a Z_2 CSL. When the effect of J_χ is small, the system is in the vicinity of the Z_2 DSL state, and naturally, it supports a Z_2 CSL wherein \mathcal{T} is explicitly broken by the J_χ term.

We argue that the Z_2 CSL state is characterized by the $\nu = 4$ state in Kitaev's sixteenfold way of anyon theories [84–86], with a chiral central charge $c = 2$. Nevertheless, the $U(1)$ CSL, which has the same topological order as the Kalmeyer-Laughlin state [67, 68], is not part of the sixteenfold way theories and has a chiral central charge $c = 1$. This distinction can be directly revealed by the topological ground-state degeneracy on a torus [87–89]. When placing the Gutzwiller projected state on the torus, four states can be constructed by changing the boundary conditions of parton mean-field Hamiltonian in both \hat{x} and \hat{y} directions. In the case of the Z_2 CSL, we have found that four states are linearly independent, forming the topologically degenerate ground-state manifold. In contrast, for the $U(1)$ CSL, we confirmed that the ground-state degeneracy is reduced to two, in agreement with the $U(1)_2$ topological order. Further details can be found in the Supplementary Material [69].

Summary— In conclusion, we revisit the J_1 - J_2 model in the paramagnetic regime by combining the Gutzwiller-guided

DMRG method and analytical analyses. By examining the ground-state energies and, particularly, the wave function fidelities, we provide direct and strong evidence that the QSL phase in the J_1 - J_2 model is a Z_2 Dirac QSL. To explore the potential topologically ordered phases in the vicinity of the Z_2 Dirac QSL, we add a spin chirality J_χ term in the J_1 - J_2 model and map out its phase diagram, where we find two distinct CSLs, i.e., Z_2 and U(1) CSLs, separated by a phase transition. With the help of PSG analysis, we find that all of the Dirac QSL and two CSLs can be efficiently described by Gutzwiller projected parton states. Apart from certain exactly solvable models, our results strongly clarify the validity of the parton construction method in a crucial and concrete model.

In addition to enhancing computational efficiency, the Gutzwiller-guided DMRG method serves as a robust and potent platform for directly evaluating various key properties, e.g., wave function fidelities. This effectively reduces the substantial finite-size effects typically encountered in numerical simulations. Meanwhile, Gutzwiller projected wave function is a versatile tool for systematically studying topological order [66, 90]. In the future, it will be interesting to prepare the

parton states in the semion sectors of Z_2 CSL by using this method, and then adiabatically evolve it by DMRG [90] to capture two different semion sectors in the J_1 - J_2 - J_χ model.

Our research could spark renewed interest in this pending issue and related problems. (i) Doping this Z_2 Dirac QSL or CSLs to explore possible superconducting states. (ii) It would be desirable to further explore topological properties such as entanglement spectra for the Z_2 CSL phase by DMRG calculations on wider cylinders, variational Monte Carlo on larger tori, and tensor network calculations in the thermodynamic limit. (iii) Our PSG analysis points out that the parameters on the 4th bonds of the parton Hamiltonian support a CSL ansatz preserving all the lattice symmetry. Whether such a CSL can emerge in the J_1 - J_2 - J_4 model through spontaneously breaking TRS is worth exploring.

Acknowledgements— We thank Francesco Ferrari for the communications on variational Monte Carlo data. H.-K. Jin acknowledges the support from the start-up funding from ShanghaiTech University. YHZ was supported by a startup fund from Johns Hopkins University and the Alfred P. Sloan Foundation through a Sloan Research Fellowship (YHZ).

-
- [1] P. W. Anderson, Mater. Res. Bull. **8**, 153 (1973), URL <http://www.sciencedirect.com/science/article/pii/0025540873901670>.
- [2] P. W. Anderson, Science **235**, 1196 (1987), URL <https://www.science.org/doi/10.1126/science.235.4793.1196>.
- [3] X. G. Wen, F. Wilczek, and A. Zee, Phys. Rev. B **39**, 11413 (1989), URL <https://link.aps.org/doi/10.1103/PhysRevB.39.11413>.
- [4] N. Read and S. Sachdev, Phys. Rev. Lett. **66**, 1773 (1991), URL <https://link.aps.org/doi/10.1103/PhysRevLett.66.1773>.
- [5] P. W. Anderson, P. A. Lee, M. Randeria, T. M. Rice, N. Trivedi, and F. C. Zhang, J. Phys.: Condens. Matter **16**, R755 (2004), URL <https://doi.org/10.1088%2F0953-8984%2F16%2F24%2Fr02>.
- [6] P. A. Lee, N. Nagaosa, and X.-G. Wen, Rev. Mod. Phys. **78**, 17 (2006), URL <https://link.aps.org/doi/10.1103/RevModPhys.78.17>.
- [7] P. A. Lee, Science **321**, 1306 (2008), URL <http://www.sciencemag.org/content/321/5894/1306.short>.
- [8] L. Balents, Nature **464**, 199 (2010), URL <http://dx.doi.org/10.1038/nature08917>.
- [9] L. Savary and L. Balents, Rep. Prog. Phys. **80**, 016502 (2016), URL <https://doi.org/10.1088/0034-4885/80/1/016502>.
- [10] Y. Zhou, K. Kanoda, and T.-K. Ng, Rev. Mod. Phys. **89**, 025003 (2017), URL <https://link.aps.org/doi/10.1103/RevModPhys.89.025003>.
- [11] J. Knolle and R. Moessner, Annu. Rev. Condens. Matter Phys. **10**, 451 (2019), URL <https://doi.org/10.1146/annurev-conmatphys-031218-013401>.
- [12] C. Broholm, R. J. Cava, S. A. Kivelson, D. G. Nocera, M. R. Norman, and T. Senthil, Science **367** (2020), ISSN 0036-8075, URL <https://science.sciencemag.org/content/367/6475/eaay0668>.
- [13] P. Chandra and B. Douçot, Phys. Rev. B **38**, 9335 (1988), URL <https://link.aps.org/doi/10.1103/PhysRevB.38.9335>.
- [14] E. Dagotto and A. Moreo, Phys. Rev. Lett. **63**, 2148 (1989), URL <https://link.aps.org/doi/10.1103/PhysRevLett.63.2148>.
- [15] S. Sachdev and R. N. Bhatt, Phys. Rev. B **41**, 9323 (1990), URL <https://link.aps.org/doi/10.1103/PhysRevB.41.9323>.
- [16] D. Poilblanc, E. Gagliano, S. Bacci, and E. Dagotto, Phys. Rev. B **43**, 10970 (1991), URL <https://link.aps.org/doi/10.1103/PhysRevB.43.10970>.
- [17] A. V. Chubukov and T. Jolicoeur, Phys. Rev. B **44**, 12050 (1991), URL <https://link.aps.org/doi/10.1103/PhysRevB.44.12050>.
- [18] H. J. Schulz and T. A. L. Ziman, Europhysics Letters **18**, 355 (1992), URL <https://dx.doi.org/10.1209/0295-5075/18/4/013>.
- [19] R. R. P. Singh, Z. Weihong, C. J. Hamer, and J. Oitmaa, Phys. Rev. B **60**, 7278 (1999), URL <https://link.aps.org/doi/10.1103/PhysRevB.60.7278>.
- [20] M. E. Zhitomirsky and K. Ueda, Phys. Rev. B **54**, 9007 (1996), URL <https://link.aps.org/doi/10.1103/PhysRevB.54.9007>.
- [21] L. Capriotti and S. Sorella, Phys. Rev. Lett. **84**, 3173 (2000), URL <https://link.aps.org/doi/10.1103/PhysRevLett.84.3173>.
- [22] K. Takano, Y. Kito, Y. Ōno, and K. Sano, Phys. Rev. Lett. **91**, 197202 (2003), URL <https://link.aps.org/doi/10.1103/PhysRevLett.91.197202>.
- [23] M. Mambri, A. Läuchli, D. Poilblanc, and F. Mila, Phys. Rev. B **74**, 144422 (2006), URL <https://link.aps.org/doi/10.1103/PhysRevB.74.144422>.
- [24] R. Darradi, O. Derzhko, R. Zinke, J. Schulenburg, S. E. Krüger, and J. Richter, Phys. Rev. B **78**, 214415 (2008), URL <https://link.aps.org/doi/10.1103/PhysRevB.78.214415>.
- [25] M. Arlego and W. Brenig, Phys. Rev. B **78**, 224415 (2008), URL <https://link.aps.org/doi/10.1103/PhysRevB.78.224415>.

- 78.224415.
- [26] J.-F. Yu and Y.-J. Kao, Phys. Rev. B **85**, 094407 (2012), URL <https://link.aps.org/doi/10.1103/PhysRevB.85.094407>.
- [27] R. L. Doretto, Phys. Rev. B **89**, 104415 (2014), URL <https://link.aps.org/doi/10.1103/PhysRevB.89.104415>.
- [28] S.-S. Gong, W. Zhu, D. N. Sheng, O. I. Motrunich, and M. P. A. Fisher, Phys. Rev. Lett. **113**, 027201 (2014), URL <https://link.aps.org/doi/10.1103/PhysRevLett.113.027201>.
- [29] S. Morita, R. Kaneko, and M. Imada, journal of the physical society of japan **84**, 024720 (2015), URL <https://doi.org/10.7566/JPSJ.84.024720>.
- [30] R. Haghshenas and D. N. Sheng, Phys. Rev. B **97**, 174408 (2018), URL <https://link.aps.org/doi/10.1103/PhysRevB.97.174408>.
- [31] L. Capriotti, F. Becca, A. Parola, and S. Sorella, Phys. Rev. Lett. **87**, 097201 (2001), URL <https://link.aps.org/doi/10.1103/PhysRevLett.87.097201>.
- [32] L. Wang, D. Poilblanc, Z.-C. Gu, X.-G. Wen, and F. Verstraete, Phys. Rev. Lett. **111**, 037202 (2013), URL <https://link.aps.org/doi/10.1103/PhysRevLett.111.037202>.
- [33] W.-J. Hu, F. Becca, A. Parola, and S. Sorella, Phys. Rev. B **88**, 060402 (2013), URL <https://link.aps.org/doi/10.1103/PhysRevB.88.060402>.
- [34] D. Poilblanc and M. Mambrini, Phys. Rev. B **96**, 014414 (2017), URL <https://link.aps.org/doi/10.1103/PhysRevB.96.014414>.
- [35] L. Wang and A. W. Sandvik, Phys. Rev. Lett. **121**, 107202 (2018), URL <https://link.aps.org/doi/10.1103/PhysRevLett.121.107202>.
- [36] W.-Y. Liu, S. Dong, C. Wang, Y. Han, H. An, G.-C. Guo, and L. He, Phys. Rev. B **98**, 241109 (2018), URL <https://link.aps.org/doi/10.1103/PhysRevB.98.241109>.
- [37] F. Ferrari, F. Becca, and J. Carrasquilla, Phys. Rev. B **100**, 125131 (2019), URL <https://link.aps.org/doi/10.1103/PhysRevB.100.125131>.
- [38] F. Ferrari and F. Becca, Phys. Rev. B **102**, 014417 (2020), URL <https://link.aps.org/doi/10.1103/PhysRevB.102.014417>.
- [39] Y. Nomura and M. Imada, Phys. Rev. X **11**, 031034 (2021), URL <https://link.aps.org/doi/10.1103/PhysRevX.11.031034>.
- [40] W.-Y. Liu, S.-S. Gong, Y.-B. Li, D. Poilblanc, W.-Q. Chen, and Z.-C. Gu, Science Bulletin **67**, 1034 (2022), ISSN 2095-9273, URL <https://www.sciencedirect.com/science/article/pii/S2095927322001001>.
- [41] W.-Y. Liu, D. Poilblanc, S.-S. Gong, W.-Q. Chen, and Z.-C. Gu, Phys. Rev. B **109**, 235116 (2024), URL <https://link.aps.org/doi/10.1103/PhysRevB.109.235116>.
- [42] H.-C. Jiang, H. Yao, and L. Balents, Phys. Rev. B **86**, 024424 (2012), URL <https://link.aps.org/doi/10.1103/PhysRevB.86.024424>.
- [43] X. Qian and M. Qin, Phys. Rev. B **109**, L161103 (2024), URL <https://link.aps.org/doi/10.1103/PhysRevB.109.L161103>.
- [44] L. Isaev, G. Ortiz, and J. Dukelsky, Phys. Rev. B **79**, 024409 (2009), URL <https://link.aps.org/doi/10.1103/PhysRevB.79.024409>.
- [45] F. Figueirido, A. Karlhede, S. Kivelson, S. Sondhi, M. Rocek, and D. S. Rokhsar, Phys. Rev. B **41**, 4619 (1990), URL <https://link.aps.org/doi/10.1103/PhysRevB.41.4619>.
- [46] N. B. Ivanov and P. C. Ivanov, Phys. Rev. B **46**, 8206 (1992), URL <https://link.aps.org/doi/10.1103/PhysRevB.46.8206>.
- [47] T. Einarsson and H. J. Schulz, Phys. Rev. B **51**, 6151 (1995), URL <https://link.aps.org/doi/10.1103/PhysRevB.51.6151>.
- [48] H. Schulz, T. Ziman, and D. Poilblanc, Journal de Physique I **6**, 675 (1996), URL <https://doi.org/10.1051/jp1:1996236>.
- [49] G.-M. Zhang, H. Hu, and L. Yu, Phys. Rev. Lett. **91**, 067201 (2003), URL <https://link.aps.org/doi/10.1103/PhysRevLett.91.067201>.
- [50] J. Sirker, Z. Weihong, O. P. Sushkov, and J. Oitmaa, Phys. Rev. B **73**, 184420 (2006), URL <https://link.aps.org/doi/10.1103/PhysRevB.73.184420>.
- [51] D. Schmalfuß, R. Darradi, J. Richter, J. Schulenburg, and D. Ihle, Phys. Rev. Lett. **97**, 157201 (2006), URL <https://link.aps.org/doi/10.1103/PhysRevLett.97.157201>.
- [52] V. Murg, F. Verstraete, and J. I. Cirac, Phys. Rev. B **79**, 195119 (2009), URL <https://link.aps.org/doi/10.1103/PhysRevB.79.195119>.
- [53] K. S. D. Beach, Phys. Rev. B **79**, 224431 (2009), URL <https://link.aps.org/doi/10.1103/PhysRevB.79.224431>.
- [54] J. Richter and J. Schulenburg, The European Physical Journal B **73**, 117 (2010), URL <https://doi.org/10.1140/epjb/e2009-00400-4>.
- [55] F. Mezzacapo, Phys. Rev. B **86**, 045115 (2012), URL <https://link.aps.org/doi/10.1103/PhysRevB.86.045115>.
- [56] Y. Qi and Z.-C. Gu, Phys. Rev. B **89**, 235122 (2014), URL <https://link.aps.org/doi/10.1103/PhysRevB.89.235122>.
- [57] C.-P. Chou and H.-Y. Chen, Phys. Rev. B **90**, 041106 (2014), URL <https://link.aps.org/doi/10.1103/PhysRevB.90.041106>.
- [58] J. Merino and A. Ralko, Phys. Rev. Res. **4**, 023122 (2022), URL <https://link.aps.org/doi/10.1103/PhysRevResearch.4.023122>.
- [59] J. Richter, R. Zinke, and D. J. Farnell, The European Physical Journal B **88**, 1 (2015), URL <https://doi.org/10.1140/epjb/e2014-50589-x>.
- [60] L. Wang, Z.-C. Gu, F. Verstraete, and X.-G. Wen, Phys. Rev. B **94**, 075143 (2016), URL <https://link.aps.org/doi/10.1103/PhysRevB.94.075143>.
- [61] D. Poilblanc, M. Mambrini, and S. Capponi, SciPost Phys. **7**, 041 (2019), URL <https://scipost.org/10.21468/SciPostPhys.7.4.041>.
- [62] S. R. White, Phys. Rev. Lett. **69**, 2863 (1992), URL <https://link.aps.org/doi/10.1103/PhysRevLett.69.2863>.
- [63] S. R. White, Phys. Rev. B **48**, 10345 (1993), URL <https://link.aps.org/doi/10.1103/PhysRevB.48.10345>.
- [64] U. Schollwöck, Ann. Phys. **326**, 96 (2011), ISSN 0003-4916, URL <http://www.sciencedirect.com/science/article/pii/S0003491610001752>.
- [65] X.-G. Wen, Phys. Rev. B **65**, 165113 (2002), URL <https://link.aps.org/doi/10.1103/PhysRevB.65.165113>.
- [66] H.-K. Jin, H.-H. Tu, and Y. Zhou, Phys. Rev. B **104**, L020409 (2021), URL <https://link.aps.org/doi/10.1103/PhysRevB.104.L020409>.
- [67] V. Kalmeyer and R. B. Laughlin, Phys. Rev. Lett. **59**, 2095 (1987), URL <http://link.aps.org/doi/10.1103/PhysRevLett.59.2095>.
- [68] V. Kalmeyer and R. B. Laughlin, Phys. Rev. B **39**, 11879 (1989), URL <http://link.aps.org/doi/10.1103/PhysRevB.39.11879>.
- [69] *See appendix for details.*
- [70] I. Affleck and J. B. Marston, Phys. Rev. B **37**, 3774 (1988), URL <https://link.aps.org/doi/10.1103/PhysRevB.37.3774>.

37. 3774.
- [71] C. Mudry and E. Fradkin, Phys. Rev. B **49**, 5200 (1994), URL <https://link.aps.org/doi/10.1103/PhysRevB.49.5200>.
- [72] H. Shackleton, A. Thomson, and S. Sachdev, Phys. Rev. B **104**, 045110 (2021), URL <https://link.aps.org/doi/10.1103/PhysRevB.104.045110>.
- [73] Y.-H. Wu, L. Wang, and H.-H. Tu, Phys. Rev. Lett. **124**, 246401 (2020), URL <https://link.aps.org/doi/10.1103/PhysRevLett.124.246401>.
- [74] H.-K. Jin, H.-H. Tu, and Y. Zhou, Phys. Rev. B **101**, 165135 (2020), URL <https://link.aps.org/doi/10.1103/PhysRevB.101.165135>.
- [75] A. M. Aghaei, B. Bauer, K. Shtengel, and R. V. Mishmash, *Efficient matrix-product-state preparation of highly entangled trial states: Weak mott insulators on the triangular lattice revisited* (2020), 2009.12435.
- [76] G. Petrica, B.-X. Zheng, G. K.-L. Chan, and B. K. Clark, Phys. Rev. B **103**, 125161 (2021), URL <https://link.aps.org/doi/10.1103/PhysRevB.103.125161>.
- [77] H.-K. Jin, R.-Y. Sun, Y. Zhou, and H.-H. Tu, Phys. Rev. B **105**, L081101 (2022), URL <https://link.aps.org/doi/10.1103/PhysRevB.105.L081101>.
- [78] A. E. Nielsen, G. Sierra, and J. I. Cirac, Nature communications **4**, 2864 (2013), URL <https://doi.org/10.1038/ncomms3864>.
- [79] D. Poilblanc, Phys. Rev. B **96**, 121118 (2017), URL <https://link.aps.org/doi/10.1103/PhysRevB.96.121118>.
- [80] J. Hasik, M. Van Damme, D. Poilblanc, and L. Vanderstraeten, Phys. Rev. Lett. **129**, 177201 (2022), URL <https://link.aps.org/doi/10.1103/PhysRevLett.129.177201>.
- [81] X.-T. Zhang, Y. Huang, H.-Q. Wu, D. N. Sheng, and S.-S. Gong, Phys. Rev. B **109**, 125146 (2024), URL <https://link.aps.org/doi/10.1103/PhysRevB.109.125146>.
- [82] J. Yang, Z. Liu, and L. Wang (2024), 2401.03434, URL <https://arxiv.org/abs/2401.03434>.
- [83] X.-G. Wen, *Quantum Field Theory of Many-Body Systems: From the Origin of Sound to an Origin of Light and Electrons* (Oxford University Press, 2007), ISBN 9780199227259, URL <https://doi.org/10.1093/acprof:oso/9780199227259.001.0001>.
- [84] A. Kitaev, Annals of Physics **321**, 2 (2006), ISSN 0003-4916, january Special Issue, URL <https://www.sciencedirect.com/science/article/pii/S0003491605002381>.
- [85] X.-Y. Song, A. Vishwanath, and Y.-H. Zhang, Phys. Rev. B **103**, 165138 (2021), URL <https://link.aps.org/doi/10.1103/PhysRevB.103.165138>.
- [86] S. Chulliparambil, U. F. P. Seifert, M. Vojta, L. Janssen, and H.-H. Tu, Phys. Rev. B **102**, 201111 (2020), URL <https://link.aps.org/doi/10.1103/PhysRevB.102.201111>.
- [87] Y. Zhang, T. Grover, and A. Vishwanath, Phys. Rev. B **84**, 075128 (2011), URL <https://link.aps.org/doi/10.1103/PhysRevB.84.075128>.
- [88] Y. Zhang, T. Grover, A. Turner, M. Oshikawa, and A. Vishwanath, Phys. Rev. B **85**, 235151 (2012), URL <https://link.aps.org/doi/10.1103/PhysRevB.85.235151>.
- [89] Y. Zhang and A. Vishwanath, Phys. Rev. B **87**, 161113 (2013), URL <https://link.aps.org/doi/10.1103/PhysRevB.87.161113>.
- [90] R.-Y. Sun, H.-K. Jin, H.-H. Tu, and Y. Zhou, npj Quantum Materials **9**, 16 (2024), URL <https://doi.org/10.1038/s41535-024-00627-5>.

**Supplementary information for
“Dirac and chiral spin liquids on spin-1/2 square-lattice Heisenberg antiferromagnet”**

Hui-Ke Jin,¹ Hong-Hao Tu,² Ya-Hui Zhang³

¹*School of Physical Science and Technology, ShanghaiTech University, Shanghai 201210, China*

²*Faculty of Physics and Arnold Sommerfeld Center for Theoretical Physics,
Ludwig-Maximilians-Universität München, 80333 Munich, Germany*

³*William H. Miller III Department of Physics and Astronomy,
Johns Hopkins University, Baltimore, Maryland, 21218, USA*

This Supplemental Material includes more details on (i) parton construction and SU(2) flux, (ii) brief projective symmetry group on the square lattice, (iii) quantum spin liquid ansatz for the J_1 - J_2 model, (iv) details on the J_1 - J_2 - J_χ model, (v) more details on density matrix renormalization group data, and (vi) topological-group state degeneracy.

I. PARTON CONSTRUCTION AND SU(2) FLUX

To demonstrate the parton construction clearly, one can use a fermionic parton field

$$\hat{F}_i \equiv \begin{pmatrix} f_{i\uparrow} & -f_{i\downarrow}^\dagger \\ f_{i\downarrow} & f_{i\uparrow}^\dagger \end{pmatrix}, \quad (6)$$

and fractionalize the spin operators in the representation such that

$$S_i^a = \frac{1}{4} \text{Tr}(\hat{F}_i^\dagger \sigma^a \hat{F}_i). \quad (7)$$

It is easy to verify that the above representation can recover the standard Abrikosov fermion representation of spins. Any right SU(2) rotation $\hat{F}_i \rightarrow \hat{F}_i G_i$, $G_i \in \text{SU}(2)$ leaves the physical spin S_i^a (and hence the spin-spin interactions) unchanged. Therefore the right rotation G_i corresponds to a gauge SU(2) rotation, which generates the SU(2) gauge structure in the parton construction method.

The parton mean-field Hamiltonian in terms of ansatz u_{ij} , which has been defined in Eq. (2) in the main text, can be explicitly written as

$$H_{MF} = \sum_{ij, s=\uparrow, \downarrow} \left[(i\chi'_{ij} + \chi_{ij}) f_{is}^\dagger f_{js} + \text{h.c.} \right] + \sum_{ij} \left[(\eta_{ij} + i\eta'_{ij}) (f_{i\uparrow}^\dagger f_{j\downarrow}^\dagger - f_{i\downarrow}^\dagger f_{j\uparrow}^\dagger) + \text{h.c.} \right]. \quad (8)$$

Two different mean-field Hamiltonians can lead to the same QSL state. We use the parton ansatz defined in Eq. (3) in the main text as an example. Restricting ourselves to the 1st NN bonds, the parton ansatz (we make $\chi_1 = \eta_1 = 1$) is

$$\mu_{i, i+\hat{x}} = \sigma^z + \sigma^x, \quad \mu_{i, i+\hat{y}} = \sigma^z - \sigma^x. \quad (9)$$

We can choose another gauge convention using the following gauge transformation

$$G_i = \sigma^z. \quad (10)$$

Then, Eq. (9) becomes

$$\mu_{i, i+\hat{x}} = \sigma^z - \sigma^x, \quad \mu_{i, i+\hat{y}} = \sigma^z + \sigma^x. \quad (11)$$

It is not difficult to verify that applying Eq. (10) to the ansatz in Eq (9) is equivalent to a C_4 lattice rotation. It indicates that Eq (9) is C_4 rotation invariant.

The type of H_{MF} (such as SU(2), U(1), and Z_2) can be characterized by the SU(2) flux defined on a closed loop with a base site [65]. For instance, denoting r_1, r_2, r_3, r_4 as for lattice sites forming a square in clockwise order, we can define a SU(2) flux on the site r_1 as

$$F_\square(r_1) = \mu_{r_1, r_2} \mu_{r_2, r_3} \mu_{r_3, r_4} \mu_{r_4, r_1}. \quad (12)$$

It is transformed under a SU(2) gauge transformation on r_1 as

$$F_\square(r_1) \rightarrow G_{r_1} F_\square(r_1) G_{r_1}^\dagger. \quad (13)$$

Therefore, the SU(2) flux does not necessarily commute with the local gauge transformation. If all nonzero SU(2) fluxes manifest as $F_\square \sim \sigma^0$, then the SU(2) gauge structure is not broken and the corresponding H_{MF} leads to a SU(2) QSL. If F_\square consists of at least one (two) of three Pauli matrices, H_{MF} describes a U(1) (Z_2) QSL.

For the Z_2 DSL, the SU(2) flux enclosed within the elementary square plaquette reads

$$F_\square(i) = \mu_{i, i+\hat{x}} \mu_{i+\hat{x}, i+\hat{x}+\hat{y}} \mu_{i+\hat{x}+\hat{y}, i+\hat{y}} \mu_{i+\hat{y}, i} = [(\chi_1^2 - \eta_1^2) \sigma^0 - 2i\chi\eta\sigma^y]^2 \sim a\sigma^0 + b\sigma^y. \quad (14)$$

Therefore, this flux breaks the SU(2) gauge symmetry into a U(1) one. Note that the above flux F_\square is only proportional to σ^0 when $\chi_1 = \eta_1$, namely, at this special point it supports an SU(2) rather than U(1) gauge symmetry. If we consider the bigger triangular plaquette, the corresponding gauge flux reads

$$F_\Delta(i) = \mu_{i, i+\hat{x}} \mu_{i+\hat{x}, i+2\hat{x}} \mu_{i+2\hat{x}, i+2\hat{x}+\hat{y}} \mu_{i+2\hat{x}+\hat{y}, i+2\hat{x}+2\hat{y}} \mu_{i+2\hat{x}+2\hat{y}, i} = (\chi_1^2 + \eta_1^2)^2 \eta_5 \sigma^x. \quad (15)$$

Since now only $\pm\sigma^0$ can commute with Eqs. (14) and (15) simultaneously, the presence of Eq. (15) further reduces the U(1) gauge symmetry into a Z_2 one. Importantly, the Z_2 DSL ansatz with a finite η_5 describes a Z_2 QSL. For the CSL ansatz,

the gauge flux enclosed within the elementary triangular plaquette is

$$F_a(i) = \mu_{i,i+\hat{x}}\mu_{i+\hat{x},i+\hat{x}+\hat{y}}\mu_{i+\hat{x}+\hat{y},i} \\ = [(\chi_1^2 - \eta_1^2)\sigma^0 - 2i\chi_1\eta_1\sigma^y]\eta_2'\sigma^y. \quad (16)$$

Thus Eqs. (16) and (14) support the same kind of gauge fluctuations.

II. PSG ON THE SQUARE LATTICE

Before discussing the projective symmetry group (PSG), we shall first clarify the symmetry group of the square lattice. We use (x, y) to denote the site of the square lattice. The translations T_x and T_y are applied as

$$(x, y) \xrightarrow{T_x} (x+1, y), \quad (x, y) \xrightarrow{T_y} (x, y+1). \quad (17)$$

The two parity symmetries, P_y and P_{xy} , indicate that

$$(x, y) \xrightarrow{P_y} (x, -y), \quad (x, y) \xrightarrow{P_{xy}} (y, x). \quad (18)$$

For simplicity of notation, we introduce a parity symmetry dubbed $P_x = P_{xy}P_yP_{xy}$ which leads to

$$(x, y) \xrightarrow{P_x} (-x, y). \quad (19)$$

The 90° rotation symmetry is given as $C_4 = P_yP_{xy}$ as

$$(x, y) \xrightarrow{P_{xy}} (y, x) \xrightarrow{P_y} (y, -x). \quad (20)$$

The above symmetric transformations lead to the algebraic relations

$$T_x T_y T_x^{-1} T_y^{-1} = 1, \quad (21a)$$

$$(P_y)^2 = (P_{xy})^2 = 1, \quad (21b)$$

$$T_x P_{xy} P_y P_{xy} T_x P_{xy} P_y P_{xy} = 1, \quad (21c)$$

$$T_y P_y T_y P_y = 1, \quad (21d)$$

$$T_x^{-1} P_{xy} T_y P_{xy} = 1, \quad (21e)$$

$$T_y^{-1} P_{xy} T_x P_{xy} = 1, \quad (21f)$$

$$(P_y P_{xy})^4 = 1. \quad (21g)$$

The above equations can give rise to corresponding algebraic PSG constraints [65], namely,

$$g_m, \dots, g_2 g_1 = 1 \implies G_{g_m}[g_m^{-1}(i)] \dots G_{g_2}[g_1(i)] G_{g_1}(i) = G_{\text{IGG}},$$

with $G_g(i)$ being the local gauge transformation for symmetry transformation g at site i , and G_{IGG} is the elements belonging to the invariance gauge group of PSG. For a U(1) QSL ansatz, the G_{IGG} is equivalent to a U(1) group, while for a Z_2 QSL ansatz, it is a Z_2 group. For a given G_{IGG} , one can obtain the algebraic PSG by solving the above algebraic PSG constraints. The parton mean-field parameters are transformed by a symmetric operation g as

$$\mu_{i,j} \xrightarrow{g} \mathcal{G}[g, \mu_{i,j}] \equiv G^g(i) \mu_{g(i),g(j)} [G^g(j)]^{-1}. \quad (22)$$

TABLE I: Lattice and projective symmetries for Z_2 DSL on the square lattice

	symmetry	PSG operation
T_x	$(x, y) \rightarrow (x+1, y)$	σ^0
T_y	$(x, y) \rightarrow (x, y+1)$	σ^0
P_y	$(x, y) \rightarrow (x, -y)$	$(-1)^{x+y} \sigma^y$
P_x	$(x, y) \rightarrow (-x, y)$	$(-1)^{x+y+1} \sigma^y$
P_{xy}	$(x, y) \rightarrow (y, x)$	$(-1)^{x+y} \sigma^x$
C_4	$(x, y) \rightarrow (y, -x)$	$-i\sigma^z$

If such a parton ansatz describes a symmetric QSL, then it requires $\mu_{i,j} \stackrel{\dagger}{=} \mathcal{G}[g, \mu_{i,j}]$.

By fixing a specific gauge of $G_{T_1}(i) = G_{T_2}(i) = \sigma^0$, the algebraic PSG supporting a Z_2 DSL ansatz is summarized in Table I. Note that we have fixed a SU(2) gauge to make Eq. (3) in the main text be translational invariant.

The PSG of Z_2 DSL also indicates that the time-reversal-symmetry must be preserved if we only include parton mean-field parameters on the bonds along the \hat{x} , \hat{y} , and $\hat{x} + \hat{y}$ directions. The P_y symmetry requires that

$$\mu_{i,i+\hat{x}} = \mathcal{G}[P_y, \mu_{i,i+\hat{x}}] \stackrel{\dagger}{=} -\sigma^y \mu_{i,i+\hat{x}} \sigma^y, \quad (23) \\ \mu_{i,i+2\hat{x}+2\hat{y}} = \mathcal{G}[P_y, i+2\hat{x}+2\hat{y}] \stackrel{\dagger}{=} \sigma^y \mu_{i,i-2\hat{x}+2\hat{y}} \sigma^y.$$

It is easy to verify that Eq. (3) in the main text satisfies Eq. (23). Note that the above constraint equations also indicate that the terms of $i\chi_1'\sigma^0 + \eta_1'\sigma^y$ should vanish in Z_2 DSL ansatz because of the P_y symmetry. Analogous constraint equations to Eq. (23) can be derived for the P_x and P_{xy} symmetries. For instance, the PSG of Z_2 DSL requires that

$$\mu_{i,i+2\hat{x}+2\hat{y}} = \mathcal{G}[P_{xy}, \mu_{i,i+2\hat{x}+2\hat{y}}] = \sigma^x \mu_{i,i+2\hat{x}+2\hat{y}} \sigma^x, \\ \mu_{i,i+2\hat{x}+2\hat{y}} = \mathcal{G}[P_y, \mu_{i,i+2\hat{x}+2\hat{y}}] = \sigma^y (\mu_{i,i-2\hat{x}+2\hat{y}})^\dagger \sigma^y, \quad (24) \\ \mu_{i,i+2\hat{x}+2\hat{y}} = \mathcal{G}[P_x, \mu_{i,i+2\hat{x}+2\hat{y}}] = \sigma^y \mu_{i,i-2\hat{x}+2\hat{y}} \sigma^y.$$

Then a straightforward calculation reveals that the time-reversal-symmetry breaking terms such as $i\chi_5'\sigma^0 + \eta_5'\sigma^y$ always vanishes on the bonds along the $\hat{x} \pm \hat{y}$ directions due to the parity symmetries.

Note that the time-reversal-symmetry-breaking terms on bonds along the other directions are in principle allowed by parity symmetries. For instance, we consider the terms on the 4th NN bonds with a general form of $\mu_{i,i+2\hat{x}+\hat{y}} = i\chi_4'\sigma^0 + \eta_4'\sigma^y$. Then the parity symmetries require

$$\mu_{i,i+2\hat{x}+\hat{y}} = \mathcal{G}[P_y, \mu_{i,i+2\hat{x}+\hat{y}}] \stackrel{\dagger}{=} -\sigma^y (\mu'_{i,i-2\hat{x}+\hat{y}})^\dagger \sigma^y, \quad (25) \\ \mu_{i,i+2\hat{x}+\hat{y}} = \mathcal{G}[P_x, \mu_{i,i+2\hat{x}+\hat{y}}] \stackrel{\dagger}{=} -\sigma^y \mu'_{i,i-2\hat{x}+\hat{y}} \sigma^y.$$

Though the imaginary hopping χ_4' should vanish due to the symmetry, the pairing term η_4' can be a finite value.

III. QSL ANSATZ FOR J_1 - J_2 MODEL

The explicit form of the Z_2 DSL ansatz is

$$\begin{aligned}
H_{Z_2\text{DSL}} = & \sum_{\langle ij \rangle} \chi_1 (f_{i,s}^\dagger f_{j,s} + f_{j,s}^\dagger f_{i,s}) \\
& + \sum_i [\eta_1 (f_{i,\uparrow}^\dagger f_{i+\hat{x},\downarrow}^\dagger + f_{i+\hat{x},\uparrow}^\dagger f_{i,\downarrow}^\dagger) + \text{H.c.}] \\
& - \sum_i \eta_1 [(f_{i,\uparrow}^\dagger f_{i+\hat{y},\downarrow}^\dagger + f_{i+\hat{y},\uparrow}^\dagger f_{i,\downarrow}^\dagger) + \text{H.c.}] \\
& + \sum_i [\eta_5 (f_{i,\uparrow}^\dagger f_{i+2\hat{x}+2\hat{y},\downarrow}^\dagger + f_{i+2\hat{x}+2\hat{y},\uparrow}^\dagger f_{i,\downarrow}^\dagger) + \text{H.c.}] \\
& - \sum_i [\eta_5 (f_{i,\uparrow}^\dagger f_{i-2\hat{x}+2\hat{y},\downarrow}^\dagger + f_{i-2\hat{x}+2\hat{y},\uparrow}^\dagger f_{i,\downarrow}^\dagger) + \text{H.c.}],
\end{aligned} \tag{26}$$

where χ_1 , η_1 , and η_5 are variational parameters. Note that η_1 on the 1st NN bond and η_5 on the 5th NN bond satisfy the $d_{x^2-y^2}$ and d_{xy} symmetries of D_4 group, respectively. After the Fourier transformation, $H_{Z_2\text{DSL}}$ becomes

$$\begin{aligned}
H_{Z_2\text{DSL}} = & (f_{\mathbf{k},\uparrow}^\dagger f_{\mathbf{k},\downarrow}^\dagger f_{-\mathbf{k},\uparrow} f_{-\mathbf{k},\downarrow}) h_{Z_2\text{DSL}}(\mathbf{k}) \begin{pmatrix} f_{\mathbf{k},\uparrow} \\ f_{\mathbf{k},\downarrow} \\ f_{-\mathbf{k},\uparrow} \\ f_{-\mathbf{k},\downarrow} \end{pmatrix}, \\
h_{Z_2\text{DSL}} = & \begin{pmatrix} S_1 & & & A_1 + A_5 \\ & S_1 & -A_1 - A_5 & \\ & -A_1 - A_5 & -S_1 & \\ A_1 + A_5 & & & -S_1 \end{pmatrix}.
\end{aligned} \tag{27}$$

Here

$$S_1(\mathbf{k}) = \chi_1 (\cos k_x + \cos k_y),$$

$$A_1(\mathbf{k}) = \eta_1 (\cos k_x - \cos k_y),$$

$$A_5(\mathbf{k}) = \eta_5 [\cos(2k_x + 2k_y) - \cos(2k_x - 2k_y)].$$

At $\mathbf{k} = (\pi/2, \pm\pi/2)$, we find that $S_1(\mathbf{k}) = A_1(\mathbf{k}) = A_5(\mathbf{k}) = 0$. Consequently, $H_{Z_2\text{DSL}}$ exhibits Dirac cones at $(\pi/2, \pi/2)$ and $(\pi/2, -\pi/2)$. A $\mathbf{k} \cdot \mathbf{p}$ expansion around the Dirac cone of $(\pi/2, \pm\pi/2)$ leads to

$$\begin{aligned}
\tilde{h}_{Z_2} = & \begin{pmatrix} f_{\mathbf{p},\uparrow}^\dagger \\ f_{-\mathbf{p},\downarrow} \end{pmatrix}^T \begin{pmatrix} \chi_1(-p_x \pm p_y) & \eta_1(-p_x \mp p_y) \mp 8\eta_5 p_x p_y \\ h.c. & -\chi_1(-p_x \pm p_y) \end{pmatrix} \begin{pmatrix} f_{\mathbf{p},\uparrow} \\ f_{-\mathbf{p},\downarrow} \end{pmatrix} \\
& + \begin{pmatrix} f_{\mathbf{p},\downarrow}^\dagger \\ f_{-\mathbf{p},\uparrow} \end{pmatrix}^T \begin{pmatrix} \chi_1(-p_x \pm p_y) & \eta_1(p_x \pm p_y) \pm 8\eta_5 p_x p_y \\ h.c. & -\chi_1(-p_x \pm p_y) \end{pmatrix} \begin{pmatrix} f_{\mathbf{p},\downarrow} \\ f_{-\mathbf{p},\uparrow} \end{pmatrix}.
\end{aligned}$$

In Table II, we list the wave function fidelity between Gutzwiller projected Z_2 DSL state and DMRG state on various cylinders.

Another possible QSL candidate is a π -flux state with the Hamiltonian as

$$\begin{aligned}
H_{SU2-\pi} = & \sum_{i,s} [(-1)^{ix} (f_{i,s}^\dagger f_{i+\hat{y},s} + f_{i+\hat{y},s}^\dagger f_{i,s})] + \\
& \sum_{i,s} [(f_{i,s}^\dagger f_{i+\hat{x},s} + f_{i+\hat{x},s}^\dagger f_{i,s})].
\end{aligned} \tag{28}$$

TABLE II: The wave function fidelity between Gutzwiller projected Z_2 DSL state and DMRG state, $F = |\langle \Psi_{Z_2\text{DSL}} | \Psi_{\text{DMRG}} \rangle|$, on various cylinders.

	F	$F^{1/L_x/L_y}$
$L_y = 4, L_x = 12$	0.9367	0.9986
$L_y = 6, L_x = 12$	0.9089	0.9987
$L_y = 8, L_x = 8$	0.9149	0.9986
$L_y = 8, L_x = 12$	0.8691	0.9985

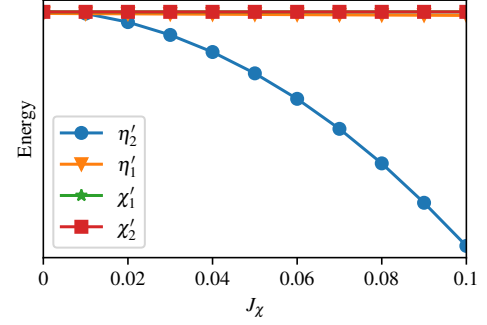


FIG. 3: The variational ground-state energies are obtained by varying parton parameters shown in the legend. The other parton parameters are fixed as $\chi_1 = 1$, $\eta_1 = 1.42$, and $\eta_5 = 0.42$. The calculations are performed on a YC6 cylinder with $L_x = 8$.

By noting that the only nonzero gauge flux on the elementary square plaquette expresses as $F \sim -\sigma^0$, the mean-field ansatz $H_{SU2-\pi}$ describes a $SU(2)$ QSL with Dirac-type spinon excitations. We use $SU(2)$ - π DSL to denote this state. However, the overlap between $SU(2)$ - π DSL parton state and the DMRG state is almost zero, which indicates that even though $SU(2)$ - π DSL also manifests Dirac cones, such an ansatz cannot efficiently describe the low-energy physics of the J_1 - J_2 model.

IV. DETAILS ON THE J_1 - J_2 - J_x MODEL

The parity symmetry of the square lattice is broken when J_x is finite. Then some PSG constraints in Eqs. (23) and (24) are removed. Consequently, the time-reversal-symmetry breaking terms with a general form of $i\chi'_n \sigma^0 + \eta_n \sigma^y$ are allowed. However, the remaining C_4 rotation symmetry requires that

$$\begin{aligned}
\mu_{i,i+\hat{x}} &= \mathcal{G}[C_4, \mu_{i,i+\hat{x}}] \stackrel{!}{=} \sigma^z (\mu_{i,i+\hat{y}})^\dagger \sigma^z, \\
\mu_{i,i+\hat{x}+\hat{y}} &= \mathcal{G}[C_4, i + \hat{x} + \hat{y}] \stackrel{!}{=} \sigma^z \mu_{i,i+\hat{x}-\hat{y}} \sigma^z.
\end{aligned} \tag{29}$$

The above constraints give rise to the CSL ansatz shown in Eq. (5) in the main text.

The CSL ansatz leads to four parton parameters, namely, $\chi'_1, \chi'_2, \eta'_1$, and η'_5 . To determine the critical parameters of the J_1 - J_2 - J_x model, we perform calculations of the variational energy by activating one of the four parameters at a time while setting the other three to zero. The results are shown in Fig. 3, which clearly demonstrates that only η'_2 , the id_{xy} pairing term

on the 2nd NN bonds, significantly contributes to the variational energy.

Focusing on η'_2 , the parton mean-field Hamiltonian becomes

$$h_{\text{CSL}} = h_{Z_2\text{DSL}} + \begin{pmatrix} 0 & & & iA_2 \\ & 0 & -iA_2 & \\ & iA_2 & 0 & \\ -iA_2 & & & 0 \end{pmatrix}, \quad (30)$$

where

$$A_2 = \eta'_2 [\cos(k_x + k_y) - \cos(k_x - k_y)].$$

To see the possible boundary zero modes, we perform the Fourier transformation only along the \hat{y} -direction. After simple calculations, we obtain a mean-field Hamiltonian in the mixed basis $f_{x,k_y,s}$ as

$$\begin{aligned} H_{\text{CSL}} = & \frac{\chi_1}{2} \sum_{x,k_y,s} \left(\cos k_y f_{x,k_y,s}^\dagger f_{x,k_y,s} + f_{x,k_y,s}^\dagger f_{x+1,k_y,s} \right) + \\ & - \frac{\chi_1}{2} \sum_{x,k_y,s} \left(\cos k_y f_{x,-k_y,s}^\dagger f_{x,-k_y,s} + f_{x+1,-k_y,s}^\dagger f_{x,-k_y,s} \right) + \\ & \frac{\eta_1}{2} \sum_{x,k_y} \left(f_{x,k_y,\uparrow}^\dagger f_{x+1,-k_y,\downarrow} + f_{x+1,k_y,\uparrow}^\dagger f_{x,-k_y,\downarrow} \right) + \\ & - \frac{\eta_1}{2} \sum_{x,k_y} \left(f_{x,k_y,\downarrow}^\dagger f_{x+1,-k_y,\uparrow} + f_{x+1,k_y,\downarrow}^\dagger f_{x,-k_y,\uparrow} \right) + \\ & - \eta_1 \sum_{x,k_y} \cos k_y \left(f_{x,k_y,\uparrow}^\dagger f_{x,-k_y,\downarrow} - f_{x,k_y,\downarrow}^\dagger f_{x,-k_y,\uparrow} \right) + \\ & i\eta_5 \sum_{x,k_y} \left[\sin 2k_y \left(f_{x,k_y,\uparrow}^\dagger f_{x+2,-k_y,\downarrow} - f_{x+2,k_y,\uparrow}^\dagger f_{x,-k_y,\downarrow} \right) \right] + \\ & - i\eta_5 \sum_{x,k_y} \left[\sin 2k_y \left(f_{x,k_y,\downarrow}^\dagger f_{x+2,-k_y,\uparrow} - f_{x+2,k_y,\downarrow}^\dagger f_{x,-k_y,\uparrow} \right) \right] + \\ & \eta'_2 \sum_{x,k_y} \left[\sin k_y \left(f_{x,k_y,\uparrow}^\dagger f_{x+1,-k_y,\downarrow} - f_{x+1,k_y,\uparrow}^\dagger f_{x,-k_y,\downarrow} \right) \right] + \\ & - \eta'_2 \sum_{x,k_y} \left[\sin k_y \left(f_{x,k_y,\downarrow}^\dagger f_{x+1,-k_y,\uparrow} - f_{x+1,k_y,\downarrow}^\dagger f_{x,-k_y,\uparrow} \right) \right] + \text{h.c.} \end{aligned}$$

The above Hamiltonian exhibits zero modes at $k_y = \pm\pi/2$. Defining $a_{x,s}^\dagger = f_{x,\pi/2,s}^\dagger$ and $b_{x,s}^\dagger = f_{x,-\pi/2,s}^\dagger$, the $\pi/2$ sector of H_{CSL} reads

$$\begin{aligned} h_{\text{CSL}}^{\pi/2} = & \frac{\chi_1}{2} \sum_{x,s} \left(a_{x,k_y,s}^\dagger a_{x+1,s} - b_{x+1,s} b_{x,s}^\dagger \right) + \\ & \sum_{x,s} \theta_s \left[\left(\frac{\eta_1}{2} + \eta'_2 \right) a_{x,s}^\dagger b_{x+1,-s}^\dagger + \left(\frac{\eta_1}{2} - \eta'_2 \right) a_{x+1,s}^\dagger b_{x,-s}^\dagger \right] + \\ & \text{h.c.}, \end{aligned}$$

where $-s$ is the inverse of spin s index and $\theta_{\uparrow(\downarrow)} = 1(-1)$. Note that $h_{\text{CSL}}^{\pi/2}$ is just the Kitaev chain when $\eta_1 = 0$. Moreover, it exhibits exact zero modes when $\eta'_2 = \chi_1/2$. However, the system also exhibits nodal points at $\mathbf{k} = (0, \pi)$ and $\mathbf{k} = (\pi, 0)$, which is not a gapped chiral spin liquid. In this case, this

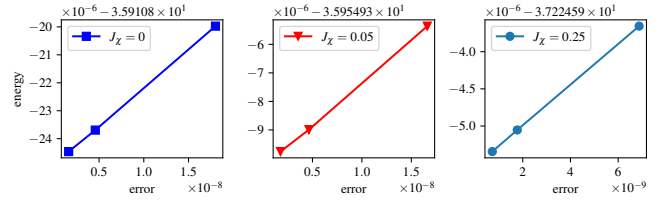


FIG. 4: Ground-state energies of the J_1 - J_2 - J_x model as functions of DMRG truncation errors. The calculations are performed on YC6 cylinders with $L_x = 12$.

parton Hamiltonian supports boundary zero modes for every k_y . When $\eta_1 > 0$, the system supports two Majorana zero modes on the boundaries of the effective 1D chain for each spin index s and each momentum $k_y = \pm\pi/2$.

V. MORE DETAILS ON DMRG DATA

To analyze the convergence of our DMRG simulations, we study the scaling behavior of the ground-state energy with the DMRG truncation errors. As shown in Fig. 4, the ground-state energy scale linearly with DMRG truncation errors for bond dimensions $\chi_D \geq 4000$, suggesting a faithful convergence in our DMRG simulations.

To see the quality of our Z_2 DSL parton ansatz, we perform DMRG simulations initialized with (i) a randomly generated product state and (ii) a Gutzwiller projected parton state, respectively. Fig. 5 shows how DMRG calculations converge with different initial states. Compared to traditional DMRG, the Gutzwiller-Boosted DMRG can shorten the convergence time to one-third. For example, the energy calculation using Gutzwiller-Boosted DMRG reaches a plateau at a wall time of approximately 6000 seconds. In contrast, conventional DMRG requires about 18000 seconds to achieve the same energy.

VI. TOPOLOGICAL GROUND-STATE DEGENERACY

The ground-state degeneracy manifests the non-trivial ground-state structure. For a topological order, its ground-state degeneracy depends on the specific geometry of the underlying lattice. Here, to investigate the difference between Gutzwiller projected Z_2 and $U(1)$ CSLs, we study the corresponding topological degeneracy on toroidal geometries.

For a general parton theory on torus, there are two distinct global fluxes, Φ_x and Φ_y , along the \hat{x} and \hat{y} directions, respectively. Overall, there are four distinct choices of those global fluxes, denoted by (Φ_x, Φ_y) . Here $\Phi_c = 0$ ($c = x, y$) for the periodic boundary condition along the \hat{c} direction and $\Phi_c = \pi$ for the antiperiodic boundary condition. Therefore, applying the Gutzwiller projection, we obtain four spin states denoted by $|\Phi_x, \Phi_y\rangle$ (e.g., $|0, 0\rangle$, $|\pi, 0\rangle$, and $|\pi, \pi\rangle$).

We then calculate the overlaps between all possible states on a $L_x = L_y = L$ torus, leading to a 4×4 overlap matrix.

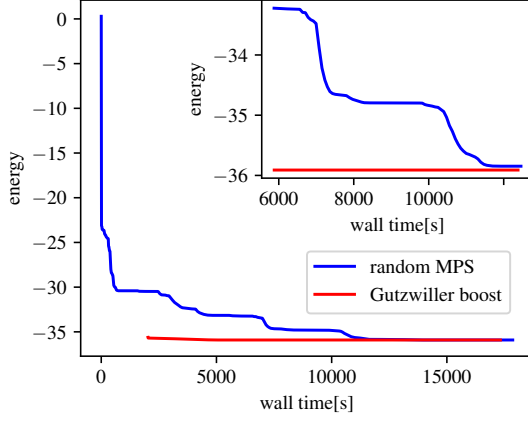


FIG. 5: The ground-state energy for a specific DMRG sweep with the total wall time cost after the sweep. The time cost of preparing a Z_2 DSL parton state at bond dimension $\chi_S = 2000$ is about 2000s. The inset shows a zoom-in plot between an interval of [~ 6000 s, ~ 12000 s]. The calculations are performed on a YC6 cylinder with $L_x = 12$ and $\chi_D = 4000$.

For small system sizes ($L = 4, 6$), we convert the Gutzwiller project state into MPSs and then calculate the overlaps directly (up to a truncation error due to the finite bond dimensions of MPS). For a larger lattice size up to $L = 16$, we use the variational Monte Carlo method to compute the overlap. Note that when using variational Monte Carlo, we first calculate the square of overlap

$$\frac{\langle \Psi_a | \Psi_b \rangle \langle \Psi_a | \Psi_b \rangle}{\langle \Psi_a | \Psi_a \rangle \langle \Psi_b | \Psi_b \rangle}. \quad (31)$$

Then, the value of overlap can be obtained by taking a square root of Eq. (31). The additional Z_2 number, which is caused by the square root, is determined by the sign of $\langle \Psi_a | \Psi_b \rangle / \langle \Psi_a | \Psi_a \rangle$.

The linearly independent ground states can be constructed by diagonalizing the 4×4 overlap matrix. For the U(1) CSL with $\eta_2 = \eta_5 = 0$ and $\eta'_2 > 0$, we find that there are only two non-zero eigenvalues of the overlap matrix, indicating a two-fold degeneracy for the U(1) CSL. For the Z_2 CSL with finite η_2 and η_5 , we find that all of those four eigenvalues are positive. Nevertheless, two of those four eigenvalues are relatively small and highly depend on the values of η_2 and η_5 . To suppress the finite-size effects, we tune (in the unit of $\chi_1 = 1$) $\eta_2 = 0.1$ and $\eta_5 = 0.6$ to enhance the Z_2 fluctuations. We also set $\eta'_2 = 0.6$ to ensure a sufficiently large chiral gap. We observe that these two smaller eigenvalues are substantially finite and exhibit no trend of decrease as the system size L grows. For instance, the two small eigenvalues are about 0.085 ± 0.002 and 0.095 ± 0.002 , respectively, for $L = 16$. Therefore, the Z_2 CSL has four-fold topologically degenerate ground states on tori.